J Soils Sediments (2014) 14:504–514
DOI 10.1007/s11368-013-0817-9

SOILS, SEC 2 • GLOBAL CHANGE, ENVIRON RISK ASSESS, SUSTAINABLE LAND USE • RESEARCH ARTICLE

In situ ATR-FTIR study on the adhesion of *Pseudomonas putida* to Red soil colloids

Huayong Wu · Wenli Chen · Xingmin Rong · Peng Cai · Ke Dai · Qiaoyun Huang

Received: 26 June 2013 / Accepted: 20 November 2013 / Published online: 3 December 2013

Abstract
Purpose Bacterial adhesion to soil particles is fundamentally important in mineral weathering, organic matter degradation, heavy metal transformation, and fate of pollutants. However, the adhesion mechanism between bacteria and soil colloids under continuous flow systems in the natural environments remains unknown.
Materials and methods The kinetics of *Pseudomonas putida* cellular adsorption and desorption on Red soil colloid films under controlled flow systems were examined using in situ attenuated total reflectance-Fourier transform infrared (ATR-FTIR) spectroscopy. Derjaguin–Landau–Verwey–Overbeek (DLVO) and non-DLVO interactions were employed to elucidate the cellular adsorption and desorption kinetics.
Results and discussion In situ ATR-FTIR spectroscopy can be used effectively to investigate the kinetics of bacterial adhesion to a soil colloid deposit. Surface proteins may be involved in the bacterial adhesion to soil colloids. The adsorption followed pseudo-first-order kinetic equation. High adsorption rate constant and great saturation coverage of adsorbed bacteria were found at high ionic strengths in dynamic systems.
Conclusions *P. putida* bacterial cellular adsorption on the soil colloid deposit was irreversible in a wide range of ionic strengths under controlled flow systems. The less reversible adhesion was probably attributed to the DLVO predicted deep secondary energy minima together with non-DLVO factors including polymer bridging, local charge heterogeneities, surface roughness, and Lewis acid–base interactions.

Keywords ATR-FTIR · Bacterial adsorption · Desorption · DVLO theory · Soil clay

Responsible editor: Hailong Wang

H. Wu · X. Rong · P. Cai · K. Dai · Q. Huang (✉)
State Key Laboratory of Agricultural Microbiology, Key Laboratory of Arable Land Conservation (Middle and Lower Reaches of Yangtze River), Ministry of Agriculture, College of Resources and Environment, Huazhong Agricultural University, Wuhan 430070, China
e-mail: qyhuang@mail.hzau.edu.cn

W. Chen
State Key Laboratory of Agricultural Microbiology, Huazhong Agricultural University, Wuhan 430070, China

1 Introduction

Soil bacteria are naturally found in a below-ground environment dominated by soil minerals and organic matter (OM). The majority of these bacteria are associated with soil particles (Nannipieri et al. 2003). Bacterial adhesion is a critical step in biofilm formation, which plays important roles in mineral weathering, aggregate turnover, OM decomposition, heavy metal transformation, and fate of organic pollutants (Kim et al. 2004; Huang et al. 2005). Furthermore, interactions between soil particles and bacteria are bidirectional. Adsorption of bacteria on soil particles widely influences the survival and biological activity of bacteria (Rong et al. 2007; Cai et al. 2013).

Bacterial adhesion to soil and sediment particles has been studied using various methods in recent years. In batch systems, *Pseudomonas putida* preferred to adsorb on the surface of goethite, followed by kaolinite and montmorillonite (Jiang et al. 2007). The notable inhibition of low molecular weight organic ligands and phosphate on *P. putida* adhesion to the above three minerals were attributed to the increased negative charges of adsorbed ligands and the competition of ligands for binding sites (Wu et al. 2011). The adhesion amount and affinity of *Bacillus subtilis* to kaolinite, montmorillonite, goethite, birnessite, quartz, and mica were primarily controlled by the specific surface areas of the minerals and the surface electrical properties, respectively (Hong et al. 2012). The cell adsorption capacity of *P. putida* and *Streptococcus suis* on soil particle size fractions ranked in the order of clay fraction > silt

fraction > sand fraction (Wu et al. 2012; Zhao et al. 2012a). The combination of batch systems with Fourier transform infrared (FTIR) spectroscopy suggested that electrostatic interactions and hydrogen bonding were mainly regarded to govern the adhesion of *P. putida* on montmorillonite, kaolinite, and goethite (Rong et al. 2008, 2010; Vasiliadou et al. 2011). Attenuated total reflectance (ATR)-FTIR spectroscopy revealed that P-OFe and COOH bonds formed upon adhesion of *Shewanella oneidensis*, *P. aeruginosa*, and *B. subtilis* cells to hematite (Parikh and Chorover 2006). Isothermal titration calorimetry addressed that electrostatic attraction may play a more vital role in the *B. subtilis* adhesion to goethite than that to kaolinite and montmorillonite (Hong et al. 2011). Nonetheless, these studies were performed in the systems that mass transport processes were not considered. In the natural environments, the dynamic reactions of microorganisms with soil reactive particles take place ubiquitously.

Deposited particle film ATR-FTIR spectroscopy is advantageous over other approaches for studying bacterial adhesion. The flow-cell ATR-FTIR spectroscopy simulated the systems that were very close to the natural environments. The soil constituents occurred as an immobile phase, while bacterial cells in a fluid were moved through the solid surface. It can readily record the information about the molecular vibrations of adsorbed bacterial cells and the kinetics of both adsorption and desorption on the same substrate in the same experiment. The high surface area obtained through micrometer-thick films of deposited particles provides good sensitivity for the spectra of adsorbed bacteria, even from a single internal reflection. Changes in the infrared (IR) peak absorbance (adsorption amount) of flowing bacterial suspensions and desorption solutions with time can be used to generate absorbance–time curves. The curves can be further used to fit absorbance corresponding to saturation coverage, adsorption, and desorption rate constants (Yong and McQuillan 2009; Shephard et al. 2010). The obtained data from the molecular vibration information, bacterial adsorption, and desorption kinetics are favorable to deduce the mechanisms of cell and soil particle binding. However, the use of the flow-cell ATR-FTIR spectroscopy in investigating the bacterial adhesion to soil components deposited on internal reflection element (IRE) is seldom reported.

The adsorption of bacteria on inert surfaces as a function of solution chemistry has recently been studied through the flow-cell ATR-FTIR spectroscopy. McWhirter et al. (2002a) found that the initial attachment (1 h) of *Pseudomonas aeruginosa* to ZnSe IRE and TiO_2 film increased up to 30 mM KCl with increasing ionic strengths (IS), but decreased at 150 mM apparently because of the charge factors and changes in the extension of bacterial surface polymers. McWhirter et al. (2002b) showed that an increase in IS from 0 to 3 mM KCl resulted in 30% increase in amide II absorbance, corresponding to a 120-nm movement of attached *P. aeruginosa* to the ZnSe surface. Shephard et al. (2010) observed that absorbance from *P. aeruginosa* attached to ZnSe intensified with increasing NaCl concentration up to 100 mM, but decreased at 300 mM because of charge screening and hydrophobicity. These studies focused on inert surfaces that are very different from surfaces exposed to bacteria in soils and sediments. As far as we know, two studies have been performed using the flow-cell ATR-FTIR technique for examining bacterial adhesion to surface-active minerals. The work of Ojeda et al. (2008) suggested that a chemical interaction is formed upon *P. putida* adhesion to hematite between the cell wall carboxylate groups and the Fe metal ions of the mineral surface. Elzinga et al. (2012) reported that P-moieties in *Shewanella putrefaciens* were preferentially adsorbed to the hematite surface through the formation of pH-dependent (pH 4.5 to 7.7) inner-sphere coordinative bonds within 24 h. Nevertheless, soil bacteria are ubiquitously exposed to soil colloids formed through cementing soil minerals and OM instead of bare minerals. To our knowledge, bacterial adhesion to soil colloids in continuous flow systems has never been addressed. The adhesion mechanism between bacteria and soil colloids under a dynamic reaction mode has not been clarified.

This work evaluated the effectivity of in situ ATR-FTIR spectroscopy in studying bacterial adhesion to soil clay fraction from an Ultisol. The mechanism of bacterial adsorption on soil colloids under controlled flow systems was also elucidated. The effect of IS on *P. putida* bacterial cellular adsorption and desorption on the soil colloid film was measured using in situ ATR-FTIR spectroscopy. The electrophoretic mobilities and hydrophobicities of bacteria and soil colloids were also examined over a wide range of IS (1 to 50 mM NaCl). Derjaguin–Landau–Verwey–Overbeek (DLVO) and non-DLVO interactions were used to explain the bacterial adsorption and desorption kinetics.

2 Materials and methods

2.1 Soil colloid

Red soil (Ultisol) was sampled from the 0~20-cm layer of a farmland at the Red Soil Experimental Station of the Chinese Academy of Agricultural Sciences, Qiyang, Hunan Province, China. The sand fractions of the soil were removed through wet sieving (48 μm). The soil colloids (<2 μm) were separated through sedimentation and were flocculated using $CaCl_2$ (0.5 mol L^{-1}) solution. The colloid suspension was repeatedly washed with ultrapure water (18.24 MΩ cm) until the electrical conductivity was below 10 μS cm^{-1}. The prepared soil colloids were oven dried at 60 °C and sieved through a 0.149-mm mesh.

The mineralogy of the soil colloids was measured through a German Bruker D8 ADVANCE X-ray diffractometer. X-ray diffraction was performed at 40 kV tube voltage and 40 mA tube current with a LynxEye detector using Ni-filtered Cu Kα

radiation, a diffracting rate of 10 min^{-1}, and step intervals of 0.02° (Xiong 1985). The mineral components of the soil colloids were kaolinite (53%), illite (39%), and vermiculite (8%). OM content was determined to be 31.0 g kg^{-1}, as analyzed through $K_2Cr_2O_7$-H_2SO_4 oxidation (Mebius 1960). The Brunauer–Emmett–Teller-specific surface area was measured via nitrogen adsorption using an Autosorb-1 standard physical adsorption analyzer (Quantachrome Autosorb-1, JEDL-6390/LV) (Emmett et al. 1938). The soil colloids were degassed at 80 °C for 3 h under vacuum prior to the adsorption measurement. The specific external surface area was 57.1 m^2 g^{-1}.

2.2 Bacterium

P. putida X4 is a Gram-negative aerobic species naturally found in soils. The strain CCTCCM209319 was preserved in the China Center for Type Culture Collection (http://www.cctcc.org/). The strain stored in 25% glycerol under −80 °C was streaked onto Luria Bertani (LB) agar slants. For each experiment, bacteria were initially inoculated into 10 mL LB medium for 7 h at 28 °C and 180 rpm to reach exponential phase with an optical density of 1.4 at 600 nm ($OD_{600\ nm}$). Then, 2 mL of the resulting bacterial suspension was transferred to 200 mL LB medium for another 14 h inoculation ($OD_{600\ nm}$=2.7) to reach mid-exponential phase. The obtained bacterial suspension was distributed over 50 mL tubes, which were centrifuged at 4,075×*g* for 10 min at 10 °C to harvest the cells. The supernatants were discarded, and the remaining bacterial pellets were washed thrice by separately resuspending the bacteria in 1, 5, 10, and 50 mM NaCl followed by centrifugation (4,075×*g*, 10 min at 10 °C). After the third wash, the wet weight of the bacterial pellets was determined. The pellets were then suspended in an appropriate volume of the corresponding NaCl solution to receive a bacterial suspension with a known cell density in terms of wet weight. The pH value of the bacterial suspension was adjusted to 5.5 using 0.1 mol L^{-1} HCl solution. A bacterial suspension with 5 mg wet weight mL^{-1} ($OD_{600\ nm}$=3.0 or 1.6×10^9 CFU mL^{-1}) was used for the ATR-FTIR experiments. Bacterial suspensions were 0.5 mg mL^{-1} ($OD_{600\ nm}$=0.3) for zeta potential and hydrodynamic radius determinations and 0.3 mg mL^{-1} ($OD_{600\ nm}$=0.18) for hydrophobicity measurements.

2.3 ATR-FTIR measurements

The ATR-FTIR spectra were recorded on a Vertex 70 spectrometer (Bruker Optik GmbH). A horizontal 45° ZnSe ATR crystal with ten reflections was coated with a soil colloid film by drying 1 mL of finely dispersed 1 mg mL^{-1} colloid suspension. The soil colloids were evenly spread across the crystal surface, resulting in a stable deposit firmly adhered to the ZnSe crystal. The coated crystal was sealed in a flow cell placed on the ATR stage inside the IR spectrometer and connected to NaCl solutions or bacterial suspensions. The bacterial suspensions were prepared using the same concentration of suspended bacteria (5 mg wet weight mL^{-1}) but with NaCl concentrations of 1, 5, 10, and 50 mM at pH 5.5. In each experiment, an appropriate NaCl solution was initially flowed over the soil colloid surface at a rate of 2 mL min^{-1} for 2 h to obtain a background spectrum. Then, bacterial adsorption was conducted by allowing the corresponding bacterial suspension to flow at the same condition for 6 h. After the adsorption, bacterial desorption was performed by flowing a proper background electrolyte for 2 h. The spectra were collected from 64 scans at 4 cm^{-1} resolution. The background spectrum consisted of the combined absorbance of the ZnSe crystal, the soil colloid deposit, and the NaCl solution. All successive spectra were subtracted from this background spectrum and smoothened. The other reference spectra of aqueous bacterial suspensions were also obtained by allowing the suspensions to flow on the ZnSe surface, from which the ZnSe and H_2O absorbance was subtracted to isolate the contributions from the microbial cells.

After subtraction and smoothening, the absorbance at approximately 1,550 cm^{-1} from the amide II band was used to depict the increase in bacterial adsorption with time. For irreversible adsorption processes under flowing suspensions with constant concentration, the variation in fractional surface coverage with time is expected to follow the equation

$$A = A_{\max}\left(1-e^{-k\,t}\right)$$

where A is the absorbance of adhered bacteria to soil colloids, $A_{\max}$ is the absorbance at saturation coverage of adhered bacteria, closely corresponding to a complete single layer of cells, k is the pseudo-first-order adsorption rate constant (second), and t is the adsorption time (Yong and McQuillan 2009). For ATR-FTIR spectroscopy adsorption experiments, the absorbance of adsorbed bacteria is proportional to the fractional surface coverage and can be used to fit kinetic data. The average distance of an adsorbed cell from the soil colloid surface is assumed to be constant with changes in coverage at constant IS.

The thickness of the soil colloid film used in the flow cell measurements was estimated at 0.7 μm, based on the amount of soil colloids on the ATR cell (1.0 mg), the dimension of the ZnSe ATR cell surface (5.11 cm^2), and an estimated density of 2.65 g cm^{-3} for the soil colloid deposit. For a 45° ZnSe ATR crystal, the penetration depth of IR light in water is 0.84 to 1.37 μm from 1,800 to 1,100 cm^{-1}, obtained after the application of the following equation:

$$d_p = \frac{\lambda}{2\pi\left(n_c^2\sin^2\alpha - n_s^2\right)^{1/2}}$$

where λ and α are the wavelength and angle of incidence, respectively. n_c (2.4) and n_s (1.33) represent the refractive indices of the ZnSe crystal and water, respectively (Harrick and du Pré 1966). Given that the soil colloid film has a refractive index higher than that of H_2O, the IR beam probes the entire thickness of the soil colloid deposit and protrudes into the aqueous phase overlying the soil colloid film. The IR evanescent wave is expected to penetrate the interior of bacterial cells adhered to soil colloid particles in the flow measurements.

2.4 Zeta potential and hydrodynamic radius detections

The bacterial suspensions used to measure the zeta potentials were prepared with 1, 5, 10, and 50 mM NaCl to make suspensions at an $OD_{600\ nm}$ of 0.3 (approximately one tenth of that used for IR experiments). The pH values of the resulting bacterial suspensions were adjusted to 5.5. Soil colloid suspensions were prepared at 0.2 mg mL^{-1} with the same concentrations of NaCl and pH value to bacterial suspensions. The soil colloid suspensions were finely dispersed by sonication for 2 min. The zeta potentials were calculated from the electrophoretic mobility according to the Smoluchowski equation. The electrophoretic mobilities and hydrodynamic radii of the bacteria and soil colloids were determined using a Zetasizer nano series (Zetasizer Nano ZS, Malvern Instruments Ltd., Malvern, Worcestershire, UK) at 25 °C.

2.5 Calculation of bacteria–soil colloid interaction energy profiles

The classic DLVO theory was chosen to elucidate the interaction energies between the bacteria and soil colloid film as a function of separation distance. Total interaction energies were quantified as the sum of van der Waals and electrostatic interactions and estimated by considering the system using the sphere–plate model. The sphere denoted bacterial cells and the plate represented the soil colloid film deposited on the ZnSe crystal. The retarded van der Waals attractive interaction energy for sphere–plate (Φ_{VDW}) system was calculated with the following expression (Gregory 1981):

$$\Phi_{VDW} = -\left(\frac{Aa_P}{6h}\right)\left[1+\left(\frac{14h}{\lambda}\right)\right]^{-1}$$

where A, a_P, and h are the Hamaker constant, bacterial cell radius (Table 1), and separation distance, respectively. λ is the characteristic wavelength (usually considered as 100 nm). The value of A was assumed to be 7.0×10^{-21} J for describing bacteria–mineral interactions in water (Hong et al. 2012).

The electrical double layer interaction energy for sphere–plate (Φ_{EDL}) system was calculated using the following equation (Bos et al. 1999):

$$\Phi_{EDL} = \pi\varepsilon_0\varepsilon_r a_P\left\{2\psi_P\psi_C\ln\left[\frac{1+\exp(-\kappa h)}{1-\exp(-\kappa h)}\right]+\left(\psi_P{}^2+\psi_C{}^2\right)\ln[1-\exp(-2\kappa h)]\right\}$$

where ε_0 denotes the permittivity of vacuum (8.85×10^{-12} C V^{-1} m^{-1}), and ε_r is the relative permittivity of water (80). ψ_P and ψ_C are the surface potentials of the cell and soil colloid, respectively. The zeta potentials are used as the approximate values instead of the surface potentials. κ represents the Debye–Hückel reciprocal length (meter). The value of κ can be determined by:

$$\kappa = \sqrt{\left(\frac{e^2\sum n_{i0}z_i^2}{\varepsilon_0\varepsilon_r k_B T}\right)}$$

where e is the electric charge (1.602×10^{-19} C). n_{i0} and z_i represent number concentration (molecules per cubic meter) and valence of ion i in bulk solution, respectively. k_B is Boltzmann constant (1.38×10^{-23} J K^{-1}), and T is the absolute temperature of the system (298 K).

2.6 Lewis acid–base property (or hydrophobicity) determinations

The adherence of bacterial cells and soil colloids to hexadecane was measured using a methodology similar to that reported elsewhere (Rosenberg et al. 1980; Bellon-Fontaine et al. 1996). A total of 4.8 mL of bacterial or soil colloid suspensions at an $OD_{600\ nm}$ of approximately 0.15, with NaCl concentrations of 1, 5, 10, and 50 mM and pH 5.5, were combined with 0.8 mL hexadecane (≥98%, Ourchem) in 10-mL centrifuge tubes. The tubes were placed on a rotating rack that stirred the tube 40 times min^{-1} end over end for 3 min and left to separate for 15 min. The hexadecane in the upper layer was removed and the $OD_{600\ nm}$ of bacterial or soil colloid suspensions in the lower layer was recorded. The percentage of adhered cells to hexadecane was calculated as:

$$\%\ \text{adherence} = (1-I/I_0)\times 100$$

Table 1 Hydrodynamic radii and electrokinetic properties of *P. putida* and soil colloids as well as calculated DLVO interaction parameters

Ionic strength (mM)	Radius of *P. putida* (μm)	Radius of soil colloids (μm)	Zeta potential of *P. putida* (mV)	Zeta potential of soil colloids (mV)	Energy barrier (k_BT)	Secondary minimum depth (k_BT)	Secondary minimum separation (nm)
1	1.60±0.05	0.19±0.01	−41.83±1.05	−34.00±1.13	2,725	−0.196	114.0
5	1.62±0.03	0.20±0.01	−41.57±1.27	−33.33±1.66	2,375	−1.285	42.0
10	1.51±0.12	0.26±0.01	−37.80±2.31	−32.10±1.31	1,758	−2.726	26.5
50	1.81±0.12	0.68±0.03	−22.50±0.35	−20.37±0.15	255	−26.135	7.0

where I_0 is the $OD_{600\ nm}$ of the bacterial or soil colloid suspensions before mixing, and I is the $OD_{600\ nm}$ after mixing.

2.7 Statistical analysis

One-way ANOVA was performed to measure statistical significance. The data are presented as mean ± standard deviation. Multiple comparisons of mean values were determined using Fisher's least significant difference test, and differences are considered significant when $p < 0.05$.

3 Results and discussion

3.1 IR spectra of soil colloids and bacterial cells

The ATR-FTIR spectrum of soil colloids is shown in Fig. 1. Bands at 1,114 and 912 cm^{-1} represented Si–O stretching (longitudinal mode) and OH deformation of inner hydroxyl groups, respectively, whereas bands at 1,028 and 1,001 cm^{-1} were assigned to the stretching of in-plane Si–O (Madejová and Komadel 2001). The strong intensities in these bands may be ascribed to the contribution of kaolinite and illite in soil colloids. The bands of OM in soil colloids were apparently covered by intense bands of clay minerals. To assess cell–soil colloid interactions, the spectra of free and soil colloid-attached bacterial cells were compared in Fig. 2. The spectra of free and adhered bacteria exhibited distinct bands at ~1,650 cm^{-1} (amide I, mainly C=O stretching), 1,550 cm^{-1} (amide II, N–H bending and C–N stretching), ~1,456 cm^{-1} (partly C–H deformation), 1,399 cm^{-1} (symmetric stretching of COO^-), ~1,242 cm^{-1} (vibrations of P=O, C–O–C, and –COOH), and ~1,085 cm^{-1} (vibrations of P–O, P=O, and C–OH) (Jiang et al. 2004). For attached cells, the bands from 1,050 to 900 cm^{-1} were disturbed by the intense absorbance of soil colloids within this range, hampering specific band assignments. Peak shifts observed in the amide bands (~1,650 and ~1,550 cm^{-1}) may reflect conformational changes of surface proteins (Parikh and Chorover 2006). Notable differences in the intensities of amide I and II bands were found between the free and soil colloid-sorbed bacterial cells.

3.2 IR analysis of bacterial adsorption and desorption kinetics

The IR absorptions in the spectral region from 1,800 to 1,100 cm^{-1} after 1, 2, 3, 4, 5, and 6 h flow of bacterial suspensions with NaCl concentrations of 1, 5, 10, and 50 mM

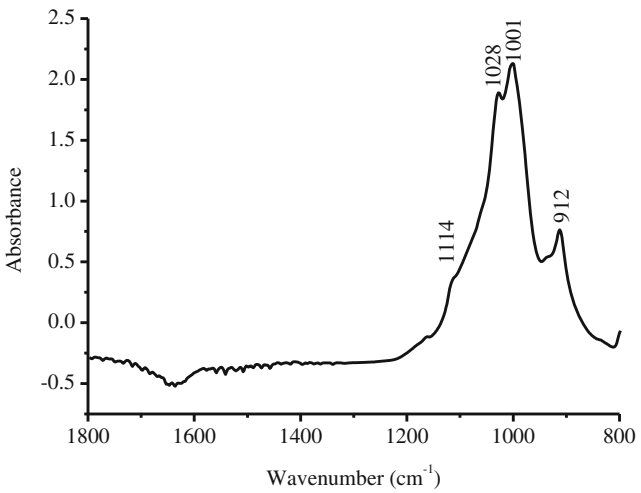

Fig. 1 ATR-FTIR spectra of soil colloids deposited on ZnSe surface at 10 mM NaCl and pH 5.5

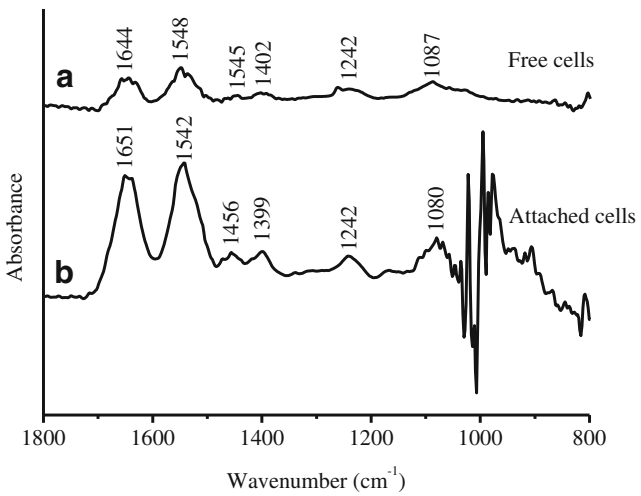

Fig. 2 ATR-FTIR spectra recorded during the flow of *P. putida* cells (1.6×10^9 CFU mL^{-1}) on the ZnSe crystal surface (**a**) and the soil colloid surface (**b**) at 10 mM NaCl and pH 5.5

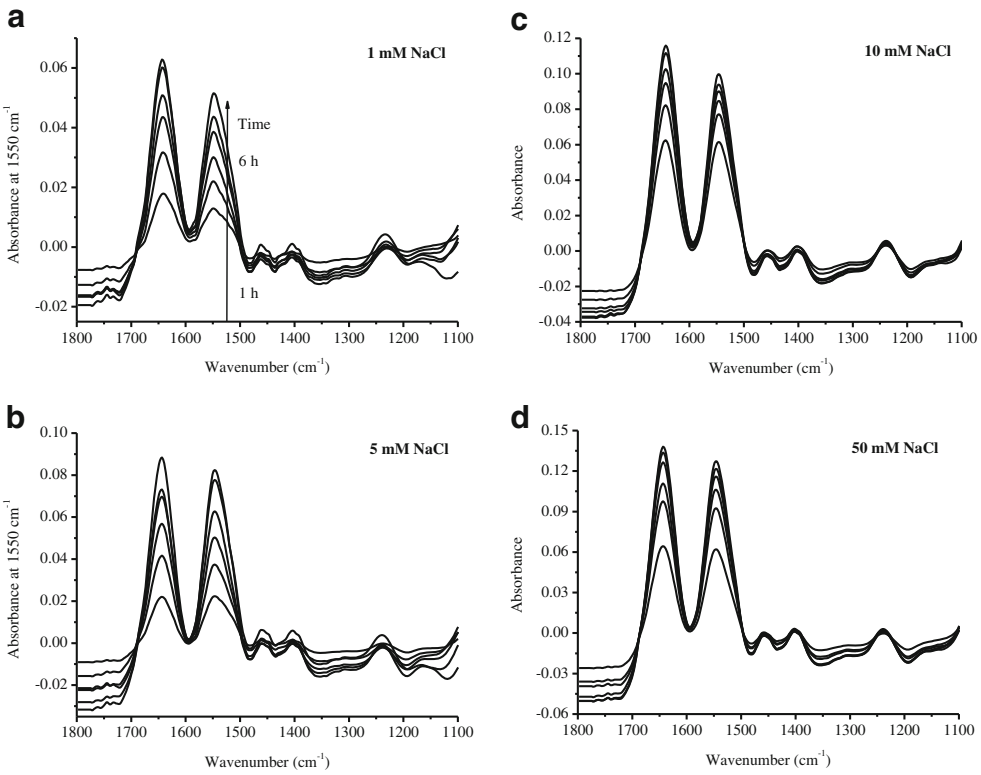

Fig. 3 Time evolution of ATR-FTIR spectra recorded during the flow of 1.6×10^9 CFU mL^{-1} *P. putida* suspension across the deposited soil colloid film on the ZnSe crystal in presence of **a** 1 mM, **b** 5 mM, **c** 10 mM, and **d** 50 mM NaCl at pH 5.5

are illustrated in Fig. 3. The shape and peak wave number of adsorbed bacteria bands were notably unchanged with various NaCl concentrations or with time. The intensities of the amide I and II bands increased rapidly at the onset of bacterial adsorption but less rapidly with prolonged time. Similar patterns were observed for all NaCl concentrations. However, the initial increasing rate of absorption and maximum absorbance varied with NaCl concentration.

Absorbance at ~1,550 cm^{-1} was used to represent the increasing bacterial coverage with time because this prominent amide II spectral band is not affected by water-related adsorptions that perturb the amide I band (Shephard et al. 2010). The changes in absorbance with time at ~1,550 cm^{-1} for all bacterial adsorption measurements are shown in Fig. 4. The absorbance–time curves varied significantly with NaCl concentration. These data showed that bacterial adhesion was remarkably impacted by IS when taking mass transport processes into account. The results displayed that bacterial absorbance was enhanced with increasing NaCl concentrations under controlled flow conditions. Although similar effects of IS on bacterial adhesion to clay minerals and goethite were reported previously in batch systems (Jiang et al. 2007), it is the first study that reported the promotion of cell adhesion to soil surface-active particles by the increase of IS in continuous flow systems. After 6 h of flowing bacterial suspension, the corresponding NaCl solution was reflowed to desorb weakly bound bacteria. The absorbance after desorption for 2 h was basically constant, indicating an irreversible adsorption process for bacterial attachment to soil colloids. The results of fitting absorbance data to the pseudo-first-order kinetic equation are listed in Table 2. The equation can reasonably fit the adsorption process based on R^2 values above 0.98. The fitted A_{max} values and adsorption rate constants (k) are independent variables and considered separately.

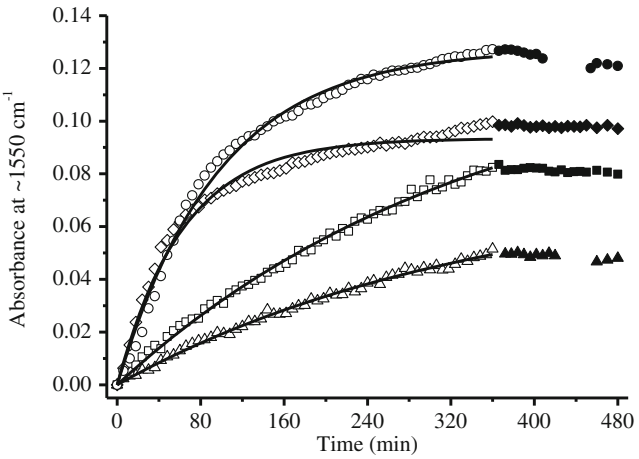

Fig. 4 Absorbance–time profiles of *P. putida* adsorbed to the deposited soil colloid from bacterial suspensions with a concentration of 1.6×10^9 CFU mL^{-1} in 1 (*triangle*), 5 (*square*), 10 (*diamond*), and 50 mM (*circle*) NaCl solutions, followed by the flow of corresponding NaCl solutions (*black triangle, black square, diamond, and black circle*). The *lines* represent the fit of the absorbance data to the irreversible adsorption relationship of $A=A_{max}(1-e^{-kt})$

Table 2 Adsorption rate parameters derived from fitting absorbance and time to $A=A_{max}(1-e^{-kt})$ for the adsorption of *P. putida* to soil colloid at different ionic strengths

NaCl (mM)	10^5 k (s^{-1})	A_{max}	R^2
1	4.9	0.076	0.995
5	4.8	0.128	0.997
10	26.6	0.093	0.982
50	17.4	0.127	0.993

A_{max} is determined by the distance between the bacterial cells and soil colloid surface as well as by the surface packing density for saturation coverage. The absorbance at *P. putida* saturation coverage on soil colloid film may correspond closely to a complete single layer of cells (Kang et al. 2006). A_{max} was found to vary considerably with NaCl concentrations as shown by the fitted data in Fig. 4. A_{max} increased from an absorbance of 0.076 to 0.127 with increasing NaCl concentration, except for the 5 mM NaCl. The change of the fitted A_{max} as influenced by IS was not entirely in agreement with that of the experimental data within 6-h adsorption time. The little disagreement may be relevant to the adsorption equilibrium time between two approaching surfaces. As shown in Fig. 4, A_{max} was achieved within 6 h at high IS (10 and 50 mM), whereas more time was needed to reach adsorption equilibrium at low IS (1 and 5 mM). Therefore, the fitted A_{max} suggests that *P. putida* cells require a prolonged time to achieve the highest adsorption capacity on the colloid film at low IS. In addition, the A_{max} values obtained in this study were much larger than that of *P. aeruginosa* attached to ZnSe crystal (Shephard et al. 2010). A_{max} values indicate that bacteria adsorbed presented greater surface packing density for saturation coverage and/or shorter separation distance to the soil colloid film than to inert surfaces. Another fitted parameter is the adsorption rate constant (k). The k value is dominated by the strength and range of interactions between the bacterial cells and soil colloid surface. The k value increased from ~5×10^5 to (17~27)$\times10^5$ s^{-1} with NaCl solutions from low to high IS. The data suggest that *P. putida* showed higher affinity to soil colloid film at higher NaCl concentrations. The adsorption and desorption data may be qualitatively explained by the classic DLVO theory and hydrophobicity in other sections.

3.3 Zeta potentials of bacteria and soil colloids

Table 1 shows that zeta potentials of bacteria and soil colloids were all negative and became less negative with higher IS. The zeta potentials of bacteria ranged from −41.83 to −22.50 mV with increasing IS from 1 to 50 mM NaCl at pH 5.5. Similarly, the zeta potentials of soil colloids varied from −34.00 to −18.43 mV. Generally, more negative charges were observed on bacterial cells than on soil colloids.

3.4 Cell–soil colloid interaction energies

The variation in the DLVO interaction energy with separation distance at different IS is illustrated in Fig. 5a and Table 1. Total energy was changed from attraction into repulsion at separation distances of 92.5 nm when bacteria approached soil colloid at 1 mM NaCl. By contrast, the separation distances turned to 32.5, 20, and 4 nm at 5, 10, and 50 mM, respectively. Huge energy barriers at ~1.0 nm were predicted for all bacterial adhesion experiments. The enormous energy barriers decreased from 2757 to 255 k_BT with NaCl concentrations from 1 to 50 mM. Similar calculated energy barriers were observed when *Streptococcus faecalis*, *Staphylococcus aureus*, *Salmonella typhimurium*, and *Escherichia coli* adhered to metal (hydroxide)-coated or uncoated sand (Truesdail et al. 1998). The predicted substantial energy barriers suggest that the bacterial cells will not irreversibly adhere in the primary

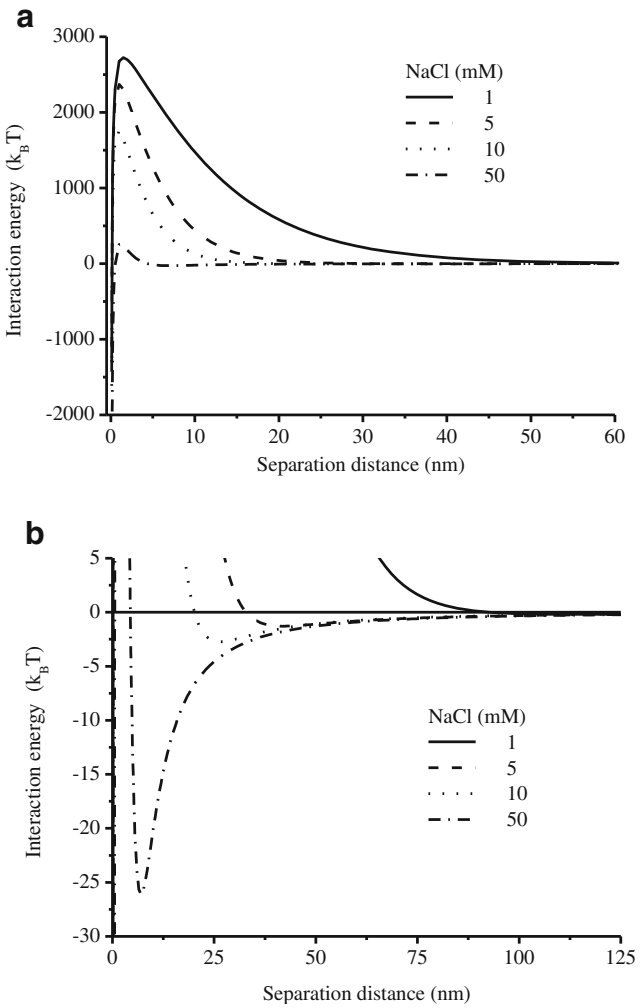

Fig. 5 Total interaction energy profiles as a function of separation distance and ionic strength between *P. putida* and soil colloid film (**a**). Identical data are replotted in the panel to highlight the secondary energy minimum (**b**)

energy minimum to the soil colloid film. However, adsorption and desorption kinetics in ATR-FTIR spectroscopy showed that the bacterial adhesion to soil colloids is an irreversible process in continuous flow systems. The irreversible adhesion may be ascribed to the presence of secondary energy minima at greater separation distance than those of the energy barriers. The DLVO profiles are replotted in Fig. 5b to emphasize the magnitude of secondary energy minima. Bacteria approaching soil colloid film would first experience attractive forces before encountering the significant repulsive energy barrier. Cells unable to overcome the energy barrier could remain associated with the soil colloid film within the secondary energy minima unless they had sufficient energy to escape (Hahn and O'Melia 2004). The irreversible adsorption process under such conditions may be attributed to the calculated deep secondary energy minima. The absolute value of the secondary minimum increased with IS. In particular, the depth of the secondary minima ranged from 0.196 k_BT at 1 mM to 26.135 k_BT at 50 mM, with corresponding separation distances of 114 and 7 nm, respectively, as listed in Table 1. Under similar IS, the depths in this study were much greater by a factor of 10 than those that existed between *E. coli* and montmorillonite or kaolinite (Zhao et al. 2012b). Given that the thermal energy of a bacterium is in the order of 0.5 k_BT (Hahn and O'Melia 2004; Redman et al. 2004), the secondary minima depths at IS not less than 5 mM shown in Table 1 should be sufficient to retain bacterial cells on the soil colloid film. The relative contribution of each force to the overall energies for the *P. putida* adhesion to the soil colloid deposit at 50 mM NaCl is illustrated in Fig. 6. The energy barrier evidently resulted from the repulsive electrostatic force, whereas the primary energy minimum at very close separation was attributed to the van der Waals force.

It is worthy to note that *P. putida* adsorption at 1 mM appeared to be somewhat inconsistent with the DLVO theory

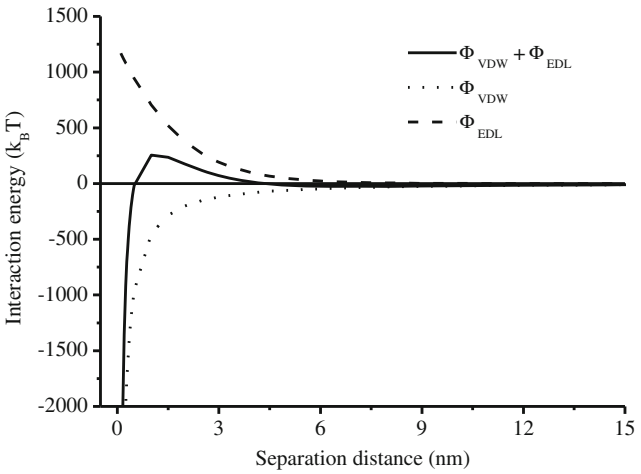

Fig. 6 DLVO theory energy profiles of the van der Waals, electrical double layer, and total interaction energies between *P. putida* and the soil colloid film at 50 mM NaCl and pH 5.5

prediction based on desorption data. The discrepancy may be due to non-DLVO factors that include (a) polymer bridging, (b) local charge heterogeneities, (c) surface roughness, and (d) Lewis acid–base interactions. These factors were not considered by the classic DLVO theory. Each of these is discussed next.

1. Polymer bridging

The surfaces of bacterial cells and soil colloids are considered to be coated by polymers. Cell surface macromolecules include lipopolysaccharides, outer membrane proteins, surface appendages (flagella, fimbriae, or pili), and extracellular polymer substances. The polymers on soil colloids are humus. Cell surface biopolymers that penetrate the electrostatic energy barrier between cells and soil colloids may cause irreversible attachment in the primary energy minimum (Rijnaarts et al. 1994; Hori and Matsumoto 2010). Cell surface macromolecular structures are often observed to extend out from the cell surfaces into solutions over distances of up to 100 nm or more (Rijnaarts et al. 1994; Touhami et al. 2006; Atabek and Camesano 2007). Even when these biopolymer tails are negatively charged, they probably span the separation (7.0–114 nm) between cell and soil colloids (Table 1). The resulting span may be attributed to the small radii of biopolymers which then are confronted with relatively small electrostatic repulsive barriers (Hori and Matsumoto 2010). Although polymers simultaneously lead to steric hindrance at some distances, it is likely that polymer bridging can partly account for the irreversible adsorption even at 1 mM NaCl.

2. Local charge heterogeneities

The surfaces of cells and soil colloids generally contain charge heterogeneities (Zhang et al. 2012). These heterogeneities provide locally favorable regions where certain bacterial cells may thus experience less repulsive or even attraction energies upon close approach, which may result in adhering in the primary energy minimum. It is possible that these bacterial cells are still retained on the soil colloids when the solution used for desorption processes is flowing.

3. Surface roughness

The DLVO theory assumes that particle surfaces are smooth. In reality, soil colloidal surfaces can be quite chemically and topographically heterogeneous. The soil colloids in this work are mainly composed of kaolinite, illite, vermiculite, and humus. Indeed, atomic force microscopy has provided evidence of the surface heterogeneity on soil colloids (Liu et al. 2003). Although a consensus has not been reached on the tendency of the effect, surface asperities have been reported to do influence

bacterial adhesion (Mitik-Dineva et al. 2009; Mei et al. 2011; Crawford et al. 2012). Interaction energy profiles are strongly impacted by surface features (Bhattacharjee et al. 1998), and the irregular surface of the soil colloids likely gives rise to a complex distribution of interaction energies. Heterogeneity in the interaction energy profiles could potentially lead to cell irreversibly attached to the soil colloids.

4. Lewis acid–base interactions

The Lewis acid–base (hydrophobicity) interaction generally is attractive and only affects bacterial adhesion to minerals at small separation distances near the primary energy minimum (Chrysikopoulos et al. 2012; Hong et al. 2012). Thus, the acid–base interaction is thought to be involved in the attachment of *P. putida* in the primary energy minimum. If polymer bridging, local charge heterogeneities, or surface roughness help *P. putida* cells adsorbed at the secondary energy minimum overcome the energy barrier, Lewis acid–base interactions begin to play an important role in the irreversible cell adhesion. The microbial adhesion to hydrocarbon assay is often conducted to determine the Lewis acid–base properties of microbial species. In this study, the percentages of cells and soil colloids adsorbed to the hexadecane droplets from solutions with 1, 5, 10, and 50 mM NaCl concentrations after 3 min of rotation are demonstrated in Fig. 7. No significant difference was found on the percentages of cells adsorbed with varied IS. However, soil colloids were found to have significantly higher adhesion percentages at 5 mM than the other conditions. To our knowledge, although it is difficult to elucidate the obtained tendency of hydrophobicity of soil colloids at different IS, the greater Lewis acid–base interaction probably contributed to the higher predicted A_{max} at 5 mM.

The findings from this work are of particular importance to geochemical ecosystems where organo-mineral complexes like soil colloids are extensively occurring. Unraveling the mechanisms and patterns of bacterial adhesion to surface-active colloids is crucial to the understanding of major biogeochemical processes including cell transport, biofilm formation, microbially mediated mobility, and transformation of metal(-loid)s in a variety of geochemical settings. The effects of other bacterial strains and environmental conditions (e.g., pH, ionic strength, organic and inorganic ligands) on cell–colloids interactions in continuous flow systems merit further study.

4 Conclusions

In situ ATR-FTIR spectroscopy has been proven to be effective in studying bacterial adhesion to a deposited soil colloid film.

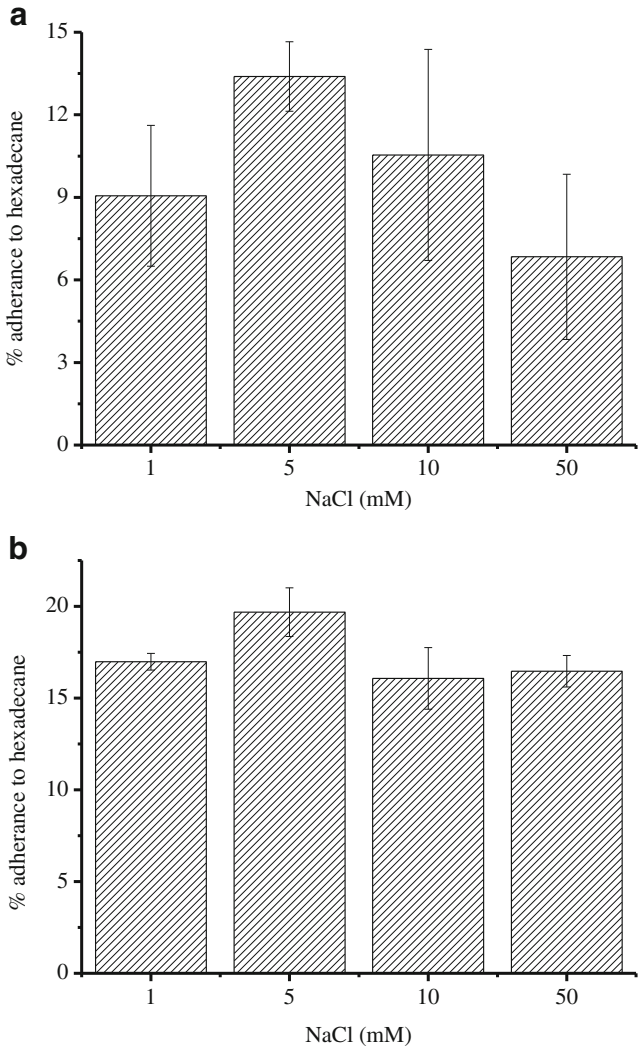

Fig. 7 Adsorption of *P. putida* cells (**a**) and soil colloids (**b**) to hexadecane from NaCl solutions with a pH of 5.5 after 3 min rotation

Changes in the protein conformation were apparently involved in the bacterial adhesion to soil colloids. The adsorption followed pseudo-first-order kinetic equation. The adsorption rate constant and saturation coverage of adsorbed cells were generally larger at higher ionic strengths. The adsorption of *P. putida* bacterial cells on the soil colloid deposit was irreversible in a wide range of ionic strengths under controlled flow systems. The less reversible adhesion may be attributed to the DLVO predicted deep secondary energy minima and non-DLVO factors including polymer bridging, local charge heterogeneities, surface roughness, and Lewis acid–base interactions.

Acknowledgments This work was kindly funded by the National Natural Science Foundation of China (40825002) and the Fundamental Research Funds for the Central Universities (2012YB17).

References

Atabek A, Camesano TA (2007) Atomic force microscopy study of the effect of lipopolysaccharides and extracellular polymers on adhesion of *Pseudomonas aeruginosa*. J Bacteriol 189:8503–8509

Bellon-Fontaine MN, Rault J, van Oss CJ (1996) Microbial adhesion to solvents: a novel method to determine the electron-donor/electron-acceptor or Lewis acid–base properties of microbial cells. Colloids Surf B 7:47–53

Bhattacharjee S, Ko CH, Elimelech M (1998) DLVO interaction between rough surfaces. Langmuir 14:3365–3375

Bos R, van der Mei HC, Busscher HJ (1999) Physico-chemistry of initial microbial adhesive interactions—its mechanisms and methods for study. FEMS Microbiol Rev 23:179–230

Cai P, Huang Q, Walker S (2013) Deposition and survival of *Escherichia coli* O157:H7 on clay minerals in a parallel plate flow system. Environ Sci Technol 47:1896–1903

Chrysikopoulos CV, Syngouna VI, Vasiliadou IA, Katzourakis VE (2012) Transport of *Pseudomonas putida* in a 3-D bench scale experimental aquifer. Transp Porous Med 94:617–642

Crawford RJ, Webb HK, Truong VK, Hasan J, Ivanova EP (2012) Surface topographical factors influencing bacterial attachment. Adv Colloid Interfac 179–182:142–149

Elzinga EJ, Huang J, Chorover J, Kretzschmar R (2012) ATR-FTIR spectroscopy study of the influence of pH and contact time on the adhesion of *Shewanella putrefaciens* bacterial cells to the surface of hematite. Environ Sci Technol 46:12848–12855

Emmett PH, Brunauer S, Love KS (1938) The measurement of surface areas of soils and soil colloids by the use of low temperature van der Waals adsorption isotherms. Soil Sci 45:57–66

Gregory J (1981) Approximate expressions for retard van der Waals interaction. J Colloid Interf Sci 83:138–145

Hahn MW, O'Melia CR (2004) Deposition and reentrainment of Brownian particles in porous media under unfavorable chemical conditions: some concepts and applications. Environ Sci Technol 38:210–220

Harrick NJ, du Pré FK (1966) Effective thickness of bulk materials and thin films for internal reflection spectroscopy. Appl Optics 5:1739–1743

Hong Z, Rong X, Cai P, Liang W, Huang Q (2011) Effects of temperature, pH and salt concentrations on the adsorption of *Bacillus subtilis* on soil clay minerals investigated by microcalorimetry. Geomicrobiol J 28:686–691

Hong Z, Rong X, Cai P, Dai K, Liang W, Chen W, Huang Q (2012) Initial adhesion of *Bacillus subtilis* on soil minerals as related to their surface properties. Eur J Soil Sci 63:457–466

Hori K, Matsumoto S (2010) Bacterial adhesion: from mechanism to control. Biochem Eng J 48:424–434

Huang PM, Wang MK, Chiu CY (2005) Soil mineral–organic matter–microbe interactions: impacts on biogeochemical processes and biodiversity in soils. Pedobiologia 49:609–635

Jiang W, Saxena A, Song B, Ward BB, Beveridge TJ, Myneni SCB (2004) Elucidation of functional groups on Gram-positive and Gram-negative bacterial surfaces using infrared spectroscopy. Langmuir 20:11433–11442

Jiang D, Huang Q, Cai P, Rong X, Chen W (2007) Adsorption of *Pseudomonas putida* on clay minerals and iron oxide. Colloids Surf B 54:217–221

Kang SY, Bremer PJ, Kim KW, McQuillan AJ (2006) Monitoring metal ion binding in single-layer *Pseudomonas aeruginosa* biofilms using ATR-IR spectroscopy. Langmuir 22:286–291

Kim J, Dong H, Seabaugh J, Newell SW, Eberl DD (2004) Role of microbes in the smectite-to-illite reaction. Science 303:830–832

Liu C, Li X, Xu F, Huang PM (2003) Atomic force microscopy of soil inorganic colloids. Soil Sci Plant Nutr 49:17–23

Madejová J, Komadel P (2001) Baseline studies of the Clay Minerals Society Source Clays: infrared meathods. Clays Clay Miner 49:410–432

McWhirter MJ, McQuillan AJ, Bremer PJ (2002a) Influence of ionic strength and pH on the first 60 min of *Pseudomonas aeruginosa* attachment to ZnSe and to TiO_2 monitored by ATR-IR spectroscopy. Colloids Surf B 26:365–372

McWhirter MJ, Bremer PJ, McQuillan AJ (2002b) Direct infrared spectroscopic evidence of pH- and ionic strength-induced changes in distance of attached *Pseudomonas aeruginosa* from ZnSe surfaces. Langmuir 18:1904–1907

Mebius LJ (1960) A rapid method for the determination of organic carbon in soil. Anal Chim Acta 22:120–124

Mei L, Busscher HJ, van der Mei HC, Ren Y (2011) Influence of surface roughness on streptococcal adhesion forces to composite resins. Dent Mater 27:770–778

Mitik-Dineva N, Wang J, Truong VK, Stoddart PR, Malherbe F, Crawford RJ, Ivanova EP (2009) Differences in colonization of five marine bacteria on two types of glass. Biofouling 25:621–631

Nannipieri P, Ascher J, Ceccherini MT, Landi L, Pietramellara G, Renella G (2003) Microbial diversity and soil functions. Eur J Soil Sci 54: 655–670

Ojeda JJ, Romero-Gonzalez ME, Pouran HM, Banwart SA (2008) In situ monitoring of the biofilm formation of *Pseudomonas putida* on hematite using flow-cell ATR-FTIR spectroscopy to investigate the formation of inner-sphere bonds between the bacteria and the mineral. Mineral Mag 72:101–106

Parikh SJ, Chorover J (2006) ATR-FTIR spectroscopy reveals bond formation during bacterial adhesion to iron oxide. Langmuir 22: 8492–8500

Redman JA, Walker SL, Elimelech M (2004) Bacterial adhesion and transport in porous media: role of the secondary energy minimum. Environ Sci Technol 38:1777–1785

Rijnaarts HHM, Norde W, Bouwer EJ, Lyklema J, Zehnder AJB (1994) Reversibility and mechanism of bacterial adhesion. Colloids Surf B 4:5–22

Rong X, Huang Q, Chen W (2007) Microcalorimetric investigation on the metabolic activity of *Bacillus thuringiensis* as influenced by kaolinite, montmorillonite and goethite. Appl Clay Sci 38:97–103

Rong X, Huang Q, He X, Chen H, Cai P, Liang W (2008) Interaction of *Pseudomonas putida* with kaolinite and montmorillonite: a combination study by equilibrium adsorption, ITC, SEM and FTIR. Colloids Surf B 64:49–55

Rong X, Chen W, Huang Q, Cai P, Liang W (2010) *Pseudomonas putida* adhesion to goethite: studied by equilibrium adsorption, SEM, FTIR and ITC. Colloids Surf B 80:79–85

Rosenberg M, Gutnick D, Rosenberg E (1980) Adherence of bacteria to hydrocarbons: a simple method for measuring cell-surface hydrophobicity. FEMS Microbiol Lett 9:29–33

Shephard JJ, Savory DM, Bremer PJ, McQuillan AJ (2010) Salt modulates bacterial hydrophobicity and charge properties influencing adhesion of *Pseudomonas aeruginosa* (PA01) in aqueous suspensions. Langmuir 26:8659–8665

Touhami A, Jericho MH, Boyd JM, Beveridge TJ (2006) Nanoscale characterization and determination of adhesion forces of *Pseudomonas aeruginosa* pili by using atomic force microscopy. J Bacteriol 188:370–377

Truesdail SE, Lukasik J, Farrah SR, Shah DO, Dickinson RB (1998) Analysis of bacterial deposition on metal (hydr)oxide-coated sand filter media. J Colloid Interf Sci 203:369–378

Vasiliadou IA, Papoulis D, Chrysikopoulos CV, Panagiotaras D, Karakosta E, Fardis M, Papavassiliou G (2011) Attachment of *Pseudomonas putida* onto differently structured kaolinite minerals: a combined ATR-FTIR and ^{1}H NMR study. Colloids Surf B 84: 354–359

Wu H, Jiang D, Cai P, Rong X, Huang Q (2011) Effects of low-molecular-weight organic ligands and phosphate on adsorption of

Pseudomonas putida by clay and iron oxide. Colloids Surf B 82: 147–151

Wu H, Jiang D, Cai P, Rong X, Dai K, Liang W, Huang Q (2012) Adsorption of *Pseudomonas putida* on soil particle size fractions: effects of solution chemisity and organic matter. J Soil Sediment 12: 143–149

Xiong Y (1985) Soil colloids, vol 2. Science Press, Beijing

Yong AG, McQuillan AJ (2009) Adsorption/desorption kinetics from ATR-FTIR spectroscopy. Aqueous oxalic acid on anatase TiO_2. Langmuir 25:3538–3548

Zhang W, Hughes J, Chen Y (2012) Impacts of hematite nanoparticle exposure on biomechanical, adhesive, and surface electrical properties of *Escherichia coli* cells. Appl Environ Microb 78:3905–3915

Zhao W, Liu X, Huang Q, Rong X, Liang W, Dai K, Cai P (2012a) Sorption of *Streptococcus suis* on various soil particles from an Alfisol and effects on pathogen metabolic activity. Eur J Soil Sci 63:558–564

Zhao W, Liu X, Huang Q, Walker SL, Cai P (2012b) Interactions of pathogens *Escherichia coli* and *Streptococcus suis* with clay minerals. Appl Clay Sci 69:37–42